PERGAMON

International Journal of Multiphase Flow 26 (2000) 1325–1350

International Journal of Multiphase Flow

www.elsevier.com/locate/ijmulflow

A random-walk simulation of thermophoretic particle deposition in a turbulent boundary layer

Chris Kröger [1], Yannis Drossinos*

European Commission, Joint Research Centre, I-21020 Ispra VA, Italy

Received 2 April 1998; received in revised form 27 July 1999

Abstract

Deposition of log-normally distributed particles in isothermal and heated turbulent boundary layers is studied via Lagrangian random-walk simulations. The velocity and temperature fields and the thermophoretic force are considered to be Gaussian random fields. Their mean values were obtained from law-of-the wall relations (velocity and temperature) and from a Knudsen number dependent expression for the thermophoretic force; their rms fluctuations were determined by polynomial fits to experimental data. The effect of aerodynamic (Saffman) lift and crossing trajectories on particle deposition is examined. We find that for particle sizes in the diffusion–impaction deposition regime the mean thermophoretic force gives the dominant contribution to total particle deposition, whereas the thermophoretic fluctuating force has only a limited contribution. The effect of lift and crossing trajectories on deposition is small with respect to the effect of the mean thermophoretic force, comparable to the effect of the fluctuating thermophoretic force, and dependent on the mean particle size. The effect of crossing trajectories (in the presence of lift) is small in isothermal flows. A limited number of particle runs was found sufficient to obtain steady-state total deposition velocities in simulations of log-normal particle-size distributions. Simulation results are compared to experimental data: we find reasonable agreement for total deposition velocity, deposited mass, and axial location of maximum deposition. © 2000 Elsevier Science Ltd. All rights reserved.

Keywords: Thermophoresis; Turbulent boundary layer; Particle deposition; Lagrangian random-walk simulation

* Corresponding author. Tel.: +39-0332-785387; fax: +39-0332-785815.
E-mail address: ioannis.drossinos@jrc.it (Y. Drossinos).
[1] Present address: Department of Atmospheric Science, University of Wyoming, Laramie, WY 82071-3038, USA.

0301-9322/00/$ - see front matter © 2000 Elsevier Science Ltd. All rights reserved.
PII: S0301-9322(99)00092-0

1. Introduction

Deposition and resuspension tests in the experimental facility STORM (Simplified Tests On Resuspension Mechanisms), De Santi et al. (1993), revealed that thermophoresis modifies considerably particle deposition in turbulent boundary layers. The understanding and modelling of the effect of thermophoresis on turbulent boundary layer particle deposition, an effect that has been considered to be simply additive to eddy impaction, is the primary aim of this work.

The STORM experiments form part of a project co-sponsored by the European Commission and ENEL, the Italian Electricity Board. These large-scale experiments investigate particle deposition and resuspension under turbulent flow conditions. The interest in thermophoretic particle deposition in turbulent boundary layers was stimulated by STORM experiments where the 10-m test pipe was thermally insulated: in this case, i.e., in the absence of a temperature gradient from the bulk flow to the wall, measurements by Krasenbrink et al. (1996) showed almost no dry-aerosol deposition. On the other hand, a post-test calculation of a deposition experiment in the presence of a temperature gradient (SD07) with a commonly used fission-product aerosol transport code, RAFT, Im et al. (1985), showed a marked increase in deposition: eddy impaction was calculated to be the dominant deposition mechanism contributing 81% of all deposition, whereas thermophoresis was responsible for the remaining 19%. One-dimensional codes such as RAFT cannot model accurately the velocity and temperature gradients near the wall, thereby crudely approximating the most important region for particle deposition. This work is an attempt to address this issue.

The approach we follow in the two-dimensional (streamwise and normal) numerical simulation is based on the work of Kallio and Reeks (1989), further extended by Zumwalt and Kallio (1990). A Lagrangian approach is taken to simulate particle motion in the turbulent boundary layer of a pipe flow and the turbulent velocity field is modelled as a field of discrete eddies with random velocities (Gaussian with an experimentally determined root mean square) and time scales (exponentially distributed). A Lagrangian random-walk (Monte-Carlo) approach was chosen instead of an Eulerian approach because it better allows the investigation of deposition processes as a function of particle sizes since overall deposition is determined by particle tracking rather than consideration of concentration gradients. Similar to the velocity decomposition into a mean and a Gaussian fluctuating component, both the temperature field and the thermophoretic force are decomposed into two components. The mean temperature across the boundary layer is given by the law-of-the wall profile, whereas the stochastic properties of the temperature field are taken to be similar to those of the velocity field in agreement with experimental observations: Finnicum and Hanratty (1985), Krishnamoorthy and Antonia (1987), and see also Lyons et al. (1991) for a comparison of experimental data on temperature fluctuations with a direct numerical simulation. We show how the mean and the fluctuating (to leading order in fluctuations) thermophoretic force are evaluated, and their contribution to particle deposition for a typical STORM experiment is analyzed.

Mean velocity values in the turbulent boundary layer are commonly modelled with the universal law-of-the-wall (Schlichting, 1979). Pipe flow and channel flow do not exactly follow the same scaling laws, particularly at low Reynolds numbers and at distances from the wall greater than $y^+ = 300$, where y^+ is the distance to the wall in wall units. Experimental

observations by Wei and Wilmarth (1989) in turbulent channel flow give a mean velocity profile which follows the logarithmic law up to the channel centre line, approximately $y^+ = 1000$. Laufer's data (Laufer, 1954), however, confirm the logarithmic velocity profile only up to a dimensionless distance from the wall of $y^+ = 300$. Both observations refer to experiments at Reynold numbers of approximately 40,000. The logarithmic law for either flow type may also differ in the von Karman constant and in the additive constant. However, for higher Reynolds numbers and for a boundary-layer thickness of about $y^+ = 200$, the regime of interest in our simulations, it is not necessary to differentiate between pipe and channel flow.

Previous numerical simulations demonstrated good agreement with experimental data for isothermal (Kallio and Reeks, 1989), and cold-wall boundary condition experiments (Zumwalt and Kallio, 1990). A calculation with hot-wall boundary conditions by Zumwalt and Kallio (1990) showed considerable underprediction of particle deposition. They argued that a detailed model for coherent turbulent structures close to the wall would improve their results. Moreover, they suggested that increasing wall roughness would lead to increased deposition. In their simulations they considered only the effect of the mean thermophoretic force, neglecting the effect of temperature fluctuations on particle deposition. Our simulation results are compared with the most frequently used isothermal test series by Liu and Agarwal (1974); as in the previously mentioned simulations our results show good agreement with their experimental data. For non-isothermal cases our results are compared to a STORM experiment and they show reasonable agreement.

A typical trajectory of a low-inertia particle in an isothermal flow field is shown in Fig. 1. It can be seen that the particle drifts very close to the wall, but in the absence of body forces, low particle inertia, or sufficient wall roughness the particle might be ejected out of the viscous sublayer into more turbulent regions. If the particle is in the tracer limit, i.e., the particle follows closely the fluid flow, particle accumulation close to the wall can only happen randomly in time, since fluid particles do not accumulate close to the wall. Yet, as a result of the numerical method which will be used to determine particle–fluid interactions, a *spurious drift* (MacInnes and Bracco, 1992), of the particles down the velocity gradient, and therefore, towards the wall, occurs. This limitation of the particle–eddy interaction model will be commented on in what follows.

Wells and Stock (1983) pointed out that in the presence of strong body forces and for particles of "sufficient" inertia the particle might cross the eddy rather than remain in it until the integral time scale of the eddy expires. This leads to an increase in particle–eddy interactions, and therefore, to faster particle diffusion. Graham and James (1996) suggested a model that considers the reduced interaction time of an inertial particle by defining the crossing time as a function of the quotient of the eddy length scale and the particle's initial velocity. Accordingly, the interaction time of a particle with a given eddy becomes the lesser of the eddy integral time scale and the crossing time. Low inertia particles, however, are not affected by the presence of body forces, and hence they are fully caught in the eddy; in this case the eddy life time defines the interaction time. We show numerically that if the finite size of the eddies is included an increase in deposition velocity is observed.

The importance of crossing trajectories due to body forces, and hence considerations of finite-size eddies, is a well known problem in atmospheric modelling, see, for example, Wilson et al. (1980, 1981). The way particle–fluid interaction is modelled results in a spurious drift that

depletes particles from high turbulence regions and accumulates them in regions of low turbulence. They argued that particle accumulation close to the wall is a consequence of the choice of the particle–eddy interaction scheme. This type of Monte-Carlo simulation is also referred to as a discontinuous random walk, since a new eddy normal fluctuating velocity is chosen only after the interaction time has been exceeded. In regions of high root mean square velocities, namely in regions of high turbulence, during one particle–eddy interaction the particle travels rather long distances down the velocity gradient. If the particle ends in a low turbulence region the probability that the particle is propelled back into regions of high fluctuating velocities is small, and therefore, the particles remain there. Whereas Wilson et al. (1980, 1981) proposed a correction to the particle equations of motion, in this work the results of Wells and Stock (1983) and Graham and James (1996) are applied and the particle–eddy interaction time is determined by considering eddies of finite extent. It is shown that the effect of crossing trajectories is non-negligible only in the presence of thermophoresis.

A second aspect of our studies is the simulation of a realistic particle-size spectrum. This could be done by simply averaging over the steady-state behaviour of each individual particle-size class, which in a particle-tracking, Lagrangian approach would require several thousand particle track calculations in each size class. Here, however, the problem is tackled by discretizing the log-normal particle-size distribution in size bins, each of which contains the same percentage of the particle distribution. This discretization leads to the calculation of a

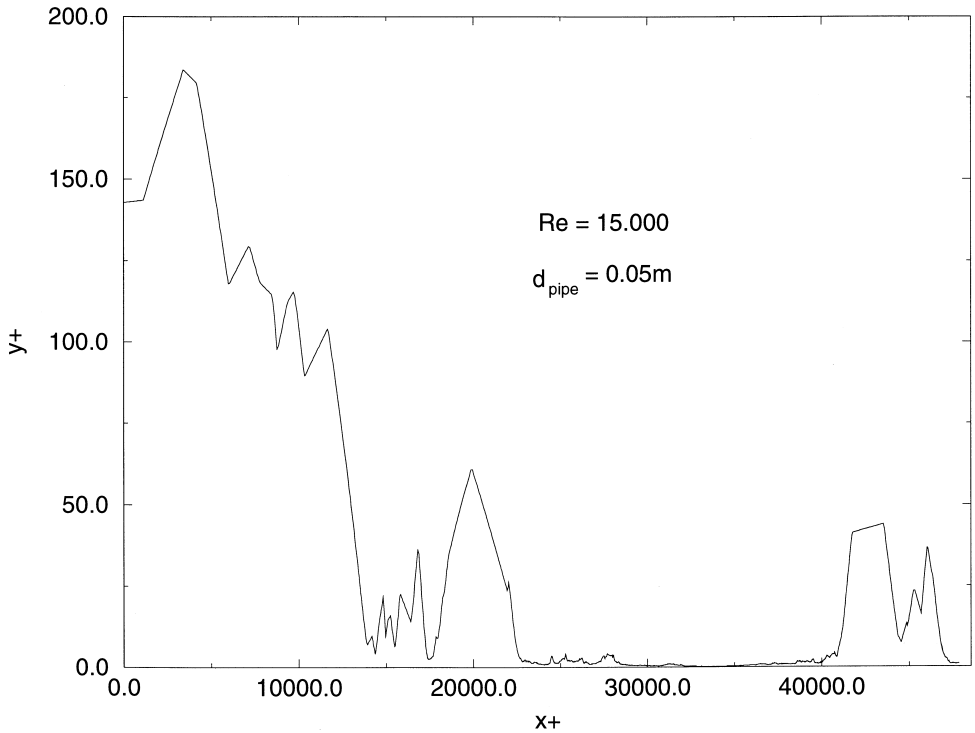

Fig. 1. Typical particle trajectory in the boundary layer of turbulent pipe flow: $\tau_p^+ = 0.02$; initial velocity $u_x^+ = 18$, $v_x^+ = 12$.

reduced number of particle tracks compared to the additive averaging. Specifically, the total number of particle tracks required to obtain steady-state deposition velocities is still in the order of tens of thousands, as usually required in Monte-Carlo simulations, but sampled from all particle-size classes.

In the next section the model is described in detail: the discretization of the particle size distribution is described, and the particle equations of motion are specified. The mean and the fluctuating components of the velocity, temperature, and thermophoretic force are presented, and the choice of the particle–eddy interaction time is described. Section 3 gives a detailed description of the numerical procedure used to solve stiff differential equations. Our numerical results are presented and discussed in Section 4, and a brief section that summarizes the results concludes the paper.

2. Model

2.1. Particle size distribution

The strongest influence on the physical behaviour of a particle of given density is its size followed by its shape. The effect of the latter may incorporated in the size distribution by introducing the aerodynamic diameter, which describes the effective diameter of a hypothetical spherical particle that would have had the same physical behaviour as the particle of irregular shape. Consequently, particle shape is not considered in this work.

One of the aims of this work is to model deposition processes of a realistic aerosol such as, for instance, the aerosol used in the STORM experiments. When the aerosol is generated its distribution can be described approximately by a log-normal probability density function. The experimentally observed spectrum covers a relatively large range of particle sizes from roughly 0.05 micron to 20 μm (Krasenbrink et al., 1996).

Most single-component aerosols are described by a log-normal cumulative distribution function F, defined as

$$F(r_p) = \int_0^{r_p} \frac{1}{r \ln \sigma_g \sqrt{2\pi}} \exp\left[- \frac{\left(\ln r - \ln r_g\right)^2}{2\left(\ln \sigma_g\right)^2} \right] dr, \tag{1}$$

where r_p is the particle radius, r_g is the geometric mean particle radius ($\ln r_g = \overline{\ln r}$), and σ_g is the geometric standard deviation [$(\ln \sigma_g)^2 = (\ln r - \ln r_g)^2$]. In the numerical simulations the distribution function is discretized by dividing the particle sizes ($r_{p,\,min}$ to $r_{p,\,max}$) into 100 size bins of size Δr_p, $i = r_p$, $i - r_p$, $i - 1$. The radii $r_{p,\,i}$ are chosen such that each size bin contain 1% of the particle distribution by numerically integrating the cumulative distribution function from $r_{p,\,i-1}$ till $r_{p,\,i}$. Accordingly only a uniformly distributed random number is necessary to select the bin number, but the resulting particle distribution is log-normal. In the discussion of the numerical methods, Section 3, it is shown that this method is more advantageous than choosing the particle size from a continuous log-normal distribution. The particle-radius

dependent properties (for example, particle relaxation time, Knudsen number, etc.) are evaluated at $r_p=(r_p,\ i+r_p,\ i+1)/2$.

For the numerical simulations the particle sizes chosen were $r_{p,\ min}=0.28$ μm and $r_{p,\ max}=13.5$ μm. We checked that the error introduced by cutting off the distribution at the low and high ends is less than 1%. The mean and the variance of the distribution are determined from experimental data, as well as the maximum particle radius.

2.2. Equations of motion

A given particle is tracked by solving its equation of motion, under the assumption that the particle does not influence the flow and that it does not interact with other particles. That is, the gas-particle system is considered dilute, and particle motion is entirely controlled by the local flow field, aerodynamic forces and body forces. The particle acceleration is be determined from Newton's second law of motion

$$\sum \boldsymbol{F}_{a,\ B}=m_p\frac{d\boldsymbol{V}}{dt}, \tag{2}$$

for constant particle mass m_p. In Eq. (2) the forces $\boldsymbol{F}_{a,\ B}$ denote aerodynamic (index a) and body forces (index B), $\boldsymbol{V}$ is the particle velocity, and t is time (bold variables refer to vectorial quantities). For incompressible flow and for particle density ρ_p greater than the fluid density $\rho_f(\rho_p\gg\rho_f)$, as well as for relatively low inertia particles, a number of external forces may be neglected such as gravity, electrical forces and Bassett's history terms. The resulting particle equation of motion is then

$$m_p\frac{d\boldsymbol{V}}{dt}=6\pi\mu r_pC_1C_2(\boldsymbol{U}-\boldsymbol{V})+\boldsymbol{F}_L+\boldsymbol{F}_B, \tag{3}$$

where μ is the fluid dynamic viscosity, C_1 the drag correction and C_2 the Cunningham slip correction to Stokes' drag law. The flow velocity is $\boldsymbol{U}$, and the last two terms are shear induced lift forces ($\boldsymbol{F}_L$) and existing body forces ($\boldsymbol{F}_B$). The first term on the right hand side is Stokes' drag law for spherical particles. The correction functions C_{1x} and C_{1y} are necessary to account for wall effects in bounded flows. An analytical expression (Happel and Brenner, 1991) to correct Stokes law for particle motion parallel and normal to the wall (x- and y-direction, respectively) is used

$$C_{1x}=\left[1-\frac{9}{16}\left(\frac{r_p}{y}\right)+\frac{1}{8}\left(\frac{r_p}{y}\right)^3-\frac{45}{256}\left(\frac{r_p}{y}\right)^4-\frac{1}{16}\left(\frac{r_p}{y}\right)^5\right]^{-1}, \tag{4}$$

$$C_{1y}=\frac{y/r_p}{y/r_p+A_0Kn-1}, \tag{5}$$

where y is the distance normal to the wall, A_0 an empirical constant taken to be 1.4, and Kn the particle Knudsen number, $Kn=\lambda/r_p$. The variable λ is the mean free path of the

surrounding fluid that can be evaluated from the viscosity expression $\lambda = \mu/(\frac{2}{\pi}\rho_f P)^{1/2}$, P being the fluid pressure (Kennard, 1938).

The Cunningham slip correction C_2, as defined in Eq. (3), is taken to be (Hinds, 1982),

$$C_2 = \left\{1 + Kn\left[1.257 + 0.4\exp(-1.1/Kn)\right]\right\}^{-1} \tag{6}$$

According to Saffman (1965,1968) the lift force on a freely rotating sphere in a uniform shear flow is

$$\boldsymbol{F}_L = 6.46\mu r_p^2(\kappa/\nu)^{1/2}(\boldsymbol{U} - \boldsymbol{V}), \tag{7}$$

where ν is the kinematic fluid viscosity and κ the local fluid velocity gradient normal to the wall. Lift and body forces are assumed to act only normal to the mean flow direction, and lift resulting from free rotation of the sphere is neglected. The importance of the aerodynamic lift force on particle deposition has been extensively studied, and the reader is referred, for example, to McLaughlin (1993), Cherukat and McLaughlin (1994), Mollinger and Nieuwstadt (1996) and Wang et al. (1997). Mollinger and Nieuwstadt (1996) measured the lift force close to the wall and found it higher than the prediction of the Saffman expression for small dimensionless particle radii. Young and Leeming (1997) argued that the lift force, and in particular Saffman lift, plays an important role in the inertia-moderated deposition regime ($\tau_p^+ > 20$, where τ_p^+ is the dimensionless particle relaxation number, cf. Eq. (11)). Wang et al. (1997) instead proposed an "optimum" lift force expression which improves agreement with experimental results on isothermal particle deposition and is approximately three times smaller than the Saffman lift. Hence, the choice of the lift force becomes important depending on the regime of dimensionless particle relaxation times that are simulated. In this work only particle deposition in the diffusion–impaction regime ($0.2 < \tau_p^+ < 20$) is analyzed, where our results suggest that the choice of the aerodynamic lift force does have an effect on particle deposition, even though it is small. Given the uncertainties associated with the choice of the lift force our choice of the Saffman force should be considered as giving an upper bound on lift-induced particle deposition.

Non-dimensionalized and decomposed in two dimensions the effect of the spanwise coordinate being assumed negligible for deposition, the particle equations of motion become

$$\frac{dv_x^+}{dt^+} = C_{1x}C_2\frac{\left(u_x^+ - v_x^+\right)}{\tau_p^+}, \tag{8}$$

$$\frac{dv_y^+}{dt^+} = C_{1y}C_2\frac{\left(u_y^+ - v_y^+\right)}{\tau_p^+} + f_L^+ + f_B^+, \tag{9}$$

with

$$f_L^+ = 0.727\left[\frac{|du_x^+/dy^+|}{(\rho_p/\rho_f)\tau_p^+}\right]^{1/2}\left(u_x^+ - v_x^+\right). \tag{10}$$

Variables have been normalized via the friction velocity u_*, and the kinematic viscosity: $y^+ = yu_*/\nu$, $x^+ = xu_*/\nu$, $u^+ = u/u_*$, $v^+ = v/u_*$, $t^+ = tu_*^2/\nu$, and $\tau_p^+ = \tau_p u_*^2/\nu$. The last quantity, the particle relaxation time τ_p, is a measure of the particle's inertia relative to the viscous drag it experiences, and it is defined as

$$\tau_p = \frac{2(\rho_p/\rho_f)r_p^2}{9\nu}. \tag{11}$$

2.3. Thermophoretic body force

In this work the normal temperature gradient from the bulk flow to the surrounding pipe walls is considered constant along the streamwise direction. In a previous work (Zumwalt and Kallio, 1990) only the effect of the mean temperature across the boundary layer on particle deposition was studied. Here, the fluctuating part of the thermophoretic force is incorporated in the calculation of particle deposition.

The thermophoretic force is expressed as

$$\boldsymbol{F}_{th} = -6\pi\mu\nu r_p K\frac{\nabla T}{T}, \tag{12}$$

where T is the fluid temperature, and K the thermophoretic coefficient. For the latter the expression proposed by Talbot et al. (1980) is used that interpolates from particle sizes in the free molecular regime to the continuum regime. The thermophoretic coefficient becomes a function of the Knudsen number and the thermal conductivities of the fluid and the particle, k_f and k_p, respectively

$$K = \frac{2C_s\left(k_f/k_p + C_t Kn\right)}{(1+3C_m Kn)\left(1+2k_f/k_p + 2C_t Kn\right)}. \tag{13}$$

For complete accommodation the coefficients are: $C_s = 1.147$ (thermal creep coefficient), $C_t = 2.2$ (temperature jump coefficient) and $C_m = 1.146$ (velocity jump coefficient).

The normalized thermophoretic force becomes

$$f_{th}^+ = \mp\frac{K}{\tau_p^+}\frac{\mathrm{d}T^+/\mathrm{d}y^+}{T_w^+ \pm T^+}, \tag{14}$$

where the normalized wall temperature T_w^+ and fluid temperature T^+ are

$$T^+ = \frac{\rho_f c_p u_* T}{0.023(k_f/D_h)Re^{4/5}Pr^m(T_b - T_w)}, \tag{15}$$

$$T_w^+ = \frac{8.65Re^{3/40}Pr^{1-n}}{|1 - T_b/T_w|}, \tag{16}$$

as suggested by Zumwalt and Kallio (1990). In Eq. (14) the top sign corresponds to a cold wall (attractive thermophoresis) and the bottom sign to a hot wall (repulsive thermophoresis). The

specific heat capacity is c_p, D_h is the hydraulic pipe diameter, T_b and T_w are bulk and wall temperature (respectively), Re the Reynolds number, $m = 0.3$ for a cold wall, $m = 0.4$ for a hot wall, and n is set to 0.02. The expression in the denominator of Eq. (15) represents a constant heat flux to the wall.

2.4. Turbulence model

The fluid velocity in the streamwise direction is described by the law of the wall in the viscous sublayer and in the logarithmic outer layer, whereas the buffer zone is interpolated by a cubic spline fit, e.g. Kallio and Reeks (1989),

$$u_x^+ = y^+ \quad y^+ \leq 5, \tag{17}$$

$$u_x^+ = a_0 + a_1 y^+ + a_2 y^{+2} + a_3 y^{+3} \quad 5 < y^+ < 30, \tag{18}$$

$$u_x^+ = 2.5 \ln y^+ + 5.5 \quad 30 \leq y^+, \tag{19}$$

where $a_0 = -1.076$, $a_1 = 1.445$, $a_2 = -0.04885$, and $a_3 = 0.0005813$.

Fluctuations are only considered normal to the wall. The r.m.s. normal velocity, u'^+_y, used here is based on the experimental measurements by Finnicum and Hanratty (1985) who suggested $u'^+ = 0.005 y^{+2}$ very close to the wall, and was later modified for the entire boundary layer by Kallio and Reeks (1989)

$$u'^+_y = \frac{0.005 y^{+2}}{1 + C\, y^{+n}} \quad 0 < y^+ < 200, \tag{20}$$

with $C = 0.002923$ and $n = 2.218$. The r.m.s. normal velocity is randomized by multiplying it by a Gaussian distributed random number of zero mean and unit variance to obtain the instantaneous eddy velocity. However, it should be noted that the assumption of a Gaussian velocity field close to the wall is questionable due to the strong shear in this region: both experimental observations and theoretical analyses (Kim et al., 1987) suggest that the distribution of the velocity field is somewhat skewed.

2.5. Time scales and interaction time

Kallio and Reeks (1989) analyzed Laufer's (1954) experimental data on energy spectra and dissipation rates within a turbulent boundary layer to obtain an expression for the eddy integral life time over the boundary layer up to $y^+ = 200$. For the region very close to the wall it was considered a constant, whereas a polynomial fit was used further away from the wall. They obtained:

$$T_L^+ = 10 \quad y^+ \leq 5, \tag{21}$$

$$T_L^+ = b_0 + b_1 y^+ + b_2 y^{+2} \quad 5 < y^+ < 200, \tag{22}$$

with $b_0 = 7.122,\ b_1 = 0.5731,\ b_2 = -0.00129$. The mean value for the time scale at a given distance from the wall is randomized by multiplying it by an exponentially distributed random number to ensure stationary turbulence. Moreover, the choice of an exponential distribution ensures the calculated dispersion of fine particles reproduces theoretical predictions (Lin and Chang, 1996).

The integral eddy length scale L^+ is assumed to be directly correlated to the Lagrangian time scale and the fluctuating velocity as follows

$$L^+ = |u_y^+| T_{\mathrm{L}}^+ N_{\mathrm{exp}}, \tag{23}$$

where u_y^+ is the instantaneous eddy velocity, obtained by randomizing the r.m.s normal velocity Eq. (20), and N_{exp} is the exponentially distributed random number that is used to define the integral time scale.

Particle–eddy interactions depend on the eddy life time, and for a high-inertia particle, also on the time required for the particle to cross an eddy. If the particle is placed in a flow field subjected to a steep temperature gradient, strong body forces will develop. The particle crossing time can then be much shorter than the life time of the eddy, and the particle will, therefore, interact with more eddies than in the absence of body forces.

If the particle is very small with no or low inertia, it is said to be in the "tracer limit" and can be considered as completely caught in the eddy. A procedure to define the case when this holds was proposed by Graham and James (1996), and it consists of the following steps. First, the ratio of the eddy length scale to the particle relaxation time, L^+/τ_{p}^+, is determined and it is compared to the particle–eddy relative velocity, $|u_{\mathrm{r}}| = |u_y^+ - v_{y,\ \mathrm{start}}^+|$, where $v_{y,\ \mathrm{start}}^+$ is the particle velocity at the beginning of the particle–eddy interaction. If $|u_y^+ - v_{y,\ \mathrm{start}}^+| < L^+/\tau_{\mathrm{p}}^+$, the particle is considered to have insufficient inertia to leave the eddy (it is caught in the eddy). Then the interaction time is the eddy life time T_{L}^+. In all other cases the particle leaves the eddy and, hence, the particle crossing time is determined to be

$$T_{\mathrm{interact}}^+ = \min\left(T_{\mathrm{cross}}^+, T_{\mathrm{L}}^+\right), \tag{24}$$

where

$$T_{\mathrm{cross}}^+ = -\tau_{\mathrm{p}}^+ \log\left(1 - \frac{L^+}{|u_{\mathrm{r}}|\tau_{\mathrm{p}}^+}\right). \tag{25}$$

Therefore, the time T_{cross}^+ is the time it takes for a given particle to cross the eddy. It becomes the particle–eddy interaction time if it is smaller than the integral time scale of the eddy. This procedure ensures that the interaction time cannot exceed the eddy life time.

2.6. Turbulent temperature field

The fluctuating fluid temperature is a passive scalar which is strongly correlated to the fluctuating normal velocity. In the spirit of the velocity decomposition, the dimensionless temperature is decomposed into a mean component, T^+, and a fluctuating component. Similar to the law-of-the-wall velocity profile the mean dimensionless temperature in the turbulent

boundary layer follows a universal profile (Hanel, 1990),

$$T^+ = Pr\, y^+ \quad y^+ \leq 5, \tag{26}$$

$$T^+ = c_0 + c_1 y^+ + c_2 y^{+2} + c_3 y^{+3} \quad 5 < y^+ < 30, \tag{27}$$

$$T^+ = 1.8 \ln y^+ + 3.8 \quad 30 < y^+, \tag{28}$$

where Pr is the fluid Prandtl number, and the appropriate constants are $c_0 = 1.28 - 2.88Pr$, $c_1 = -0.54 + 2.21Pr$, $c_2 = 0.0628 - 0.138Pr$ and $c_3 = -0.00117 + 0.00224Pr$. As for the buffer zone of the velocity profile, the temperature buffer region was fitted with a cubic spline.

Tanimoto and Hanratty (1963) measured temperature fluctuations close to a wall in fully developed turbulent pipe flow for small heat fluxes at the wall. They compared their results to Laufer's (1954)) energy data and observed a strong similarity between velocity and temperature fluctuations, both in magnitude and in their dependence on the distance to the wall. In agreement with this observation, the stochastic properties of the instantaneous temperature field are taken to be *identical* to the stochastic properties of the velocity field. In the numerical simulations described in the following section the y-dependence of the r.m.s. temperature fluctuations, T'^+, is taken to be

$$T'^+ = \frac{0.005 y^{+2}}{1 + C\, y^{+n}}, \tag{29}$$

where the constants C and n are those used in Eq. (20). Similarly to the randomization of the velocity field, this r.m.s. value is then multiplied by the Gaussian distributed random number chosen for the velocity field. The instantaneous temperature field is then determined by adding the randomized r.m.s. fluctuating temperature to the mean temperature.

Considerations of temperature fluctuations render the thermophoretic force a fluctuating quantity. In the spirit of the decomposition of all fluctuating quantities into a mean and a Gaussian distributed r.m.s. quantity the normalized thermophoretic force is decomposed as follows:

$$f^+_{\mathrm{th}} = \overline{f^+_{\mathrm{th}}} + f'^+_{\mathrm{th}}, \tag{30}$$

where, as before, the first term on the right hand side is the mean thermophoretic force and the second term is its randomized r.m.s. value. The fluctuating thermophoretic force is evaluated by expanding the term $1/T$ in Eq. (14) to leading order in fluctuations. This expansion gives, to leading order in fluctuations,

$$\overline{f^+_{\mathrm{th}}} = \mp \frac{K}{\tau^+_{\mathrm{p}}} \frac{\mathrm{d}T^+/\mathrm{d}y^+}{T^+_{\mathrm{w}} \pm T^+}, \tag{31}$$

$$f'^+_{\mathrm{th}} = \mp \frac{K}{\tau^+_{\mathrm{p}}} \frac{\mathrm{d}T'^+/\mathrm{d}y^+}{T^+_{\mathrm{w}} \pm T^+}, \tag{32}$$

where the quantity $\mathrm{d}T'^{+}/\mathrm{d}y^{+}$ is defined to be the r.m.s. temperature gradient fluctuation. The thermophoretic force expressions are derived under the assumption that the particle response times to the stable, mean temperature field and to the fluctuating temperature are equal.

Therefore, the determination of the instantaneous thermophoretic force requires values for the r.m.s. temperature gradient. Krishnamoorthy and Antonia (1987) derived data on the instantaneous temperature derivatives in a turbulent boundary layer from their measurements and they provide figures with the distribution of mean square values of temperature derivatives across the boundary layer. By means of a fourth-order spline fit through their derived data we obtained the following expression for the spatial variation of the r.m.s. temperature derivative across the boundary layer:

$$\frac{\mathrm{d}T'^{+}}{\mathrm{d}y^{+}} = d_0 + d_1 y^{+} + d_2 y^{+2} + d_3 y^{+3} + d_4 y^{+4}, \tag{33}$$

where the fitted parameters are $d_0 = 1.9806$, $d_1 = -0.052494$, $d_2 = 0.00061411$, $d_3 = -3.1216 \times 10^{-6}$, and $d_4 = 5.6856 \times 10^{-9}$. As before, the instantaneous fluctuating thermophoretic force is obtained by randomizing its r.m.s. value. In Fig. 2 the dependence of the r.m.s. temperature derivative and the r.m.s. temperature on the dimensionless distance to

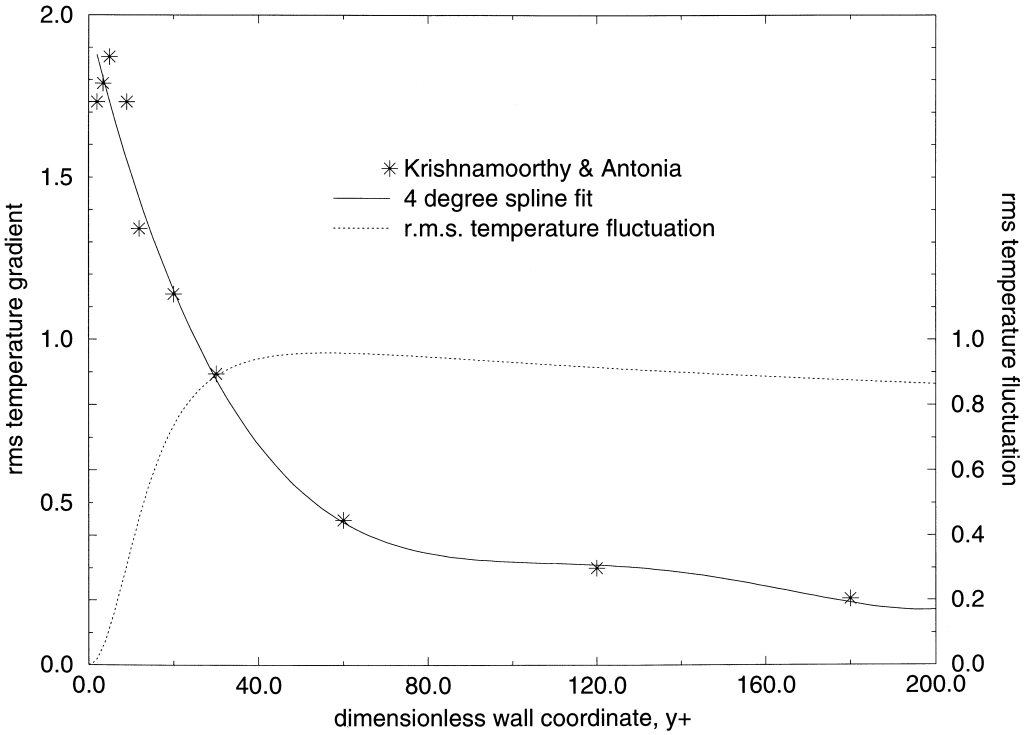

Fig. 2. The r.m.s. temperature fluctuations and r.m.s. temperature gradient fluctuations in a turbulent boundary layer.

the wall is shown. The fitting functions Eqs. (29), (33) and the experimental data of Krishnamoorthy and Antonia (1987) are plotted.

3. Numerical procedure

At the beginning of a run the discrete particle-size log-normal distribution is determined as described in Section 2.1. The particle radii $r_{\mathrm{p},\,i}$ that define the size bins are stored in an array so that the numerical integration of the cumulative distribution function is performed only once at the start of the calculation. This method, which leads to a discrete particle size distribution, is preferred to sampling particle radii from a continuous distribution not only for reduced cpu usage, but mainly because it allows easy processing of the results, i.e. particles can be easily counted in the appropriate size bins. In all reported simulations 100 size bins had been chosen. A uniform random number is then used to pick the size-bin number containing a random particle size. Afterwards, the Lagrangian eddy time scale, the eddy integral length scale, the fluctuating velocity, the fluctuating temperature and the mean velocity and temperature at this random starting position are chosen, as previously described.

The particle is released at the entrance of the pipe at a random position uniformly distributed over the boundary layer. The initial position is also recorded by dividing the boundary layer into 56 parallel y size bins. These y-bins are narrow close to the wall, where the position of particles is stored every 0.2 wall units, and their size increases to ten wall units further away from the wall. This very fine discretized mesh requires a higher number of particle trajectories in order to obtain good statistics, but it allows a precise localization of the peak of maximum particle number concentration. Given the particle position at release, the initial values for the integration can be calculated, and the particle crossing time through the eddy is defined. Following Reeks (1977) the initial particle normal velocity is chosen according to the ratio $\tau_{\mathrm{p}}^{+}/T_{\mathrm{L}}^{+}$ as follows

$$v_y^{+} = \frac{u_y^{+}}{\left(1+\tau_{\mathrm{p}}^{+}/T_{\mathrm{L}}^{+}\right)^{1/2}}. \tag{34}$$

The initial streamwise particle velocity is set to two thirds of the mean fluid velocity. Random numbers describing the eddy are kept constant over the entire particle–eddy interaction time, while the mean and r.m.s. velocity and temperature values vary depending on the distance of the particle to the wall. The particle position is determined after several integration steps, with step sizes determined by the integration routine. The time integration for both temperature and velocity is possible since the time scales for temperature and velocity fluctuations are taken to be equal. At desired streamwise "stations" particle data are recorded. The stations are distributed approximately uniformly over the pipe length, for instance at $x^{+} = 2000$, 5000, 10,000, 15,000, etc. An additional pipe section is added at the beginning of the pipe to ensure steady-state condition at the entrance.

The numerical integration scheme is based on the Bulirsch-Stoer method (Press et al., 1995). In this method, a relatively large step size is chosen that is then repeatedly subdivided and an extrapolation function is evaluated to a theoretical step size $h = 0$. The polynomial function

extrapolates the results of a finite number of subdivisions to infinite number of steps. Additionally an even error function is chosen, allowing the polynomial function extrapolation to be in terms of the variable h^2.

Since the integration routine uses an adaptive stepsize the recorded positions are not precisely at the predefined distances, but particles are recorded as soon they have passed the station. Particle positions are stored at the stations, until either the particle deposits or leaves the pipe. If a particle leaves the top y-bin through the upper limit at $y^+ = 200$, it is returned into the boundary layer at the position of its exit with opposite velocity. If a particle deposits the location (x-section) is stored and its mass is added to the mass of previously deposited particles to determine the total mass deposited in that x-section. A new particle of random size is then released at the entrance with a new random initial normal position, and the procedure is repeated.

After several thousands of particle tracks have been recorded the data are analysed. The number of calculated particle tracks is such that the quantity of interest (e.g., concentration profile, Eq. (35), or deposition velocity, Eq. (36)) attain steady-state values. Concentration profiles are calculated for each station in the following way:

$$c_i = \frac{N_i\, y^+_{200}}{N_{\text{stat}}\left(y^+_i - y^+_{i-1}\right)}, \tag{35}$$

where c_i is the normalized concentration in i-th y-bin, N_i is the number of particles passing through this y-bin, and N_{stat} is the number of all particles passing the station. The variable y^+_{200} is taken as the maximum wall region thickness (in our case $y^+_{200} = 200$), and y^+_i is the distance from the wall of the upper bound of the ith y-bin.

The deposition velocity in a given x-section is calculated as suggested by Zumwalt and Kallio (1990) and also used by Liu and Agarwal (1974)

$$V^+_{\text{dep}}(x^+) = \frac{y^+_{200} U^+_{\text{ave}}}{L^+(x^+)} \ln\left(\frac{N_{\text{in}}}{N_{\text{out}}}\right), \tag{36}$$

where $V^+_{\text{dep}}(x^+)$ is the normalized deposition velocity in the x-section, U^+_{ave} is the mean velocity between $0 < y^+ < 200$, $L^+(x^+)$ is the section length, and N_{in}, N_{out} are the number of particles entering and leaving the section, respectively. Results are mainly presented in terms of deposition velocities, and for the cases where a particle-size spectrum is simulated the total steady-state deposition velocity is presented.

Particle size distributions are recorded at the entrance of the pipe and at the exit. Since at the entrance the particles are uniformly distributed over all size bins, the particles counted at the pipe exit have to be normalized by the size-bin width, i.e., $\Delta r_{\text{p},\,i}$ as follows (Hinds, 1982),

$$f(r_{\text{p},\,i}) = \frac{N_{r_{\text{p},\,i}}}{r_{\text{p},\,i} - r_{\text{p},\,i-1}}. \tag{37}$$

Due to the narrow extent of the y-bins close to the wall, a high sampling rate is necessary to obtain good statistics, in particular to obtain smooth concentration profiles.

4. Results and discussion

The aims of the numerical simulations presented in this section are: (1) to ensure that the code reproduces well known results and experimental data under isothermal conditions; (2) to quantify the effect of the mean thermophoretic force on total particle deposition and on particle concentration close to the wall; (3) to study the influence of a fluctuating thermophoretic force on these two quantities; (4) to study the the effect of crossing trajectories in the presence and absence of body forces (thermophoresis); and (5) to estimate what constitutes a statistically sufficiently large number of particle tracks to simulate a log-normal particle-size distribution.

Data from the Liu and Agarwal (1974) isothermal experiments were used to check the performance of the code under isothermal conditions. These tests had been performed in a simple geometry under well defined flow conditions with smooth pipe walls. Particle resuspension was negligible because olive-oil droplets, which stick reasonably well onto the glass pipe walls, were used. The simulated steady-state dimensionless deposition velocities are compared to experimental data in Fig. 3. For each test case 20,000 particle tracks were calculated. There is a slight overprediction for particle sizes in the diffusion–impaction regime ($0.2 < \tau_p^+ < 10$), whereas a tiny underprediction may be noted in the inertia-moderated regime ($20 < \tau_p^+$). Wang et al. (1997) argued that this overprediction is a consequence of the Saffman

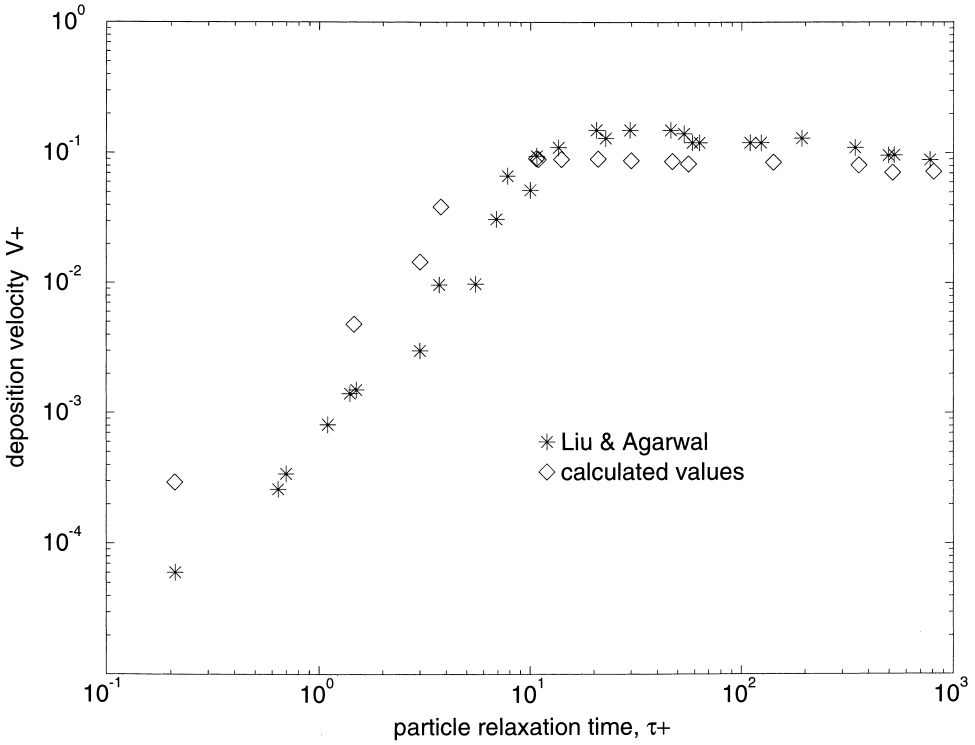

Fig. 3. Comparison of Liu and Agarwal's isothermal tests with numerical simulation.

lift, whereas their proposed smaller "optimum" force improves agreement. Nevertheless, the results compare reasonably well to experimental data, and the change in slope with increasing particle relaxation time is reproduced. These results are in agreement with previous Monte-Carlo simulations of isothermal particle deposition (Kallio and Reeks, 1989).

A series of simulations of an experiment with a temperature gradient across the turbulent boundary layer were performed. The experimental data for the material properties, the pipe geometry, and thermal hydraulic conditions, based on the experimental conditions of STORM experiment SD07, are shown in Table 1. The particle-size distribution was chosen to be log-normal with $r_g = 1.5$ μm and $\sigma_g = 1.5278$, corresponding to a minimum and maximum particle relaxation time of $\tau_p^+ \approx 0.05$ and $\tau_p^+ \approx 110$, respectively. Hence, most particles are in the diffusion–impaction deposition regime. The results of these simulations are shown in Figs. 4 and 5: total (summed over all particle sizes) steady-state deposition velocities are plotted as functions of axial position.

A number of sensitivity calculations grouped in two sets (one in the presence of a thermophoretic force, Figs. 4, and one in its absence, Fig. 5) were performed. In these the effect of particle crossing trajectories and aerodynamic lift was studied, the base case being the simulation of thermophoretic deposition only.

From Figs. 4 and 5 it becomes clear that the temperature gradient has the dominant effect on deposition velocity. In particular, comparison of Figs. 4 and 5 reveals an approximate 25-fold increase in deposition velocity for a temperature difference of 113 K. The importance of the mean thermophoretic force on particle deposition was also noted in Zumwalt and Kallio (1990) and in Thakurta et al. (1998).

The simulations shown in Fig. 4 were performed with a mean particle radius $r_g = 1.5$ μm. Accordingly, most particles do not have sufficient inertia to leave the eddy before it is dissipated, therefore, the effect of crossing trajectories is minor. However, the combination of lift and finite-size eddies has a stronger effect on particle deposition than subjecting the particles to each one separately. The effect of crossing trajectories (in the presence of a lift force) is particularly small in the absence of thermophoresis, Fig. 5. Under isothermal conditions lift increases deposition, while additional inclusion of finite-size eddies results in a negligible change of the total deposition velocity. Therefore, the consideration of finite-size eddies seems advisable in the presence of a thermophoretic force; under isothermal conditions (and for the particle relaxation times under consideration) the effect of crossing trajectories in the presence of lift is negligible. It should be noted, however, that these conclusions are based on small changes of steady-state deposition velocities, approximately 3–5%.

Table 1
SD07 experiment: main experimental conditions during the deposition phase

Carrier/quench gas	Steam/N_2	Wall temperature	490°C
Aerosol	Tin dioxide	Bulk temperature	603°C
Particle density	1611 kg/m^3	Mean centerline velocity	24.7 m/s
Particle heat conductivity	17.28 W/(mK)	Reynolds number	24,000
Prandtl number	0.986	Fluid viscosity	56.6×10^{-6} m^2/s

A clear demonstration of the effect of crossing trajectories can be seen in a simulation with $r_g = 10$ μm, shown in Fig. 6. The effect of crossing trajectories clearly exceeds the influence of lift, leading to an increase in steady-state deposition velocity of approximately 15%. This is due to increased particle–eddy interactions: in the presence of thermophoresis a particle crosses the eddy earlier, hence, it encounters more eddies increasing its effective diffusion. If finite-size eddies are not considered, lift does lead to a marked increase in deposition velocity. This observation, however, should be considered approximate given the uncertainties associated to the application of Saffman lift close to the wall. When the effects of lift and finite-size eddies are combined, the resulting deposition velocity is not merely the sum of deposition velocities due to lift and finite-size eddies. As shown in Figs. 4–6 the effects of lift and finite-sized eddies are not additive.

Simulations using different temperature gradients across the boundary layer show a similar effect of crossing trajectories. In Fig. 7 we show two simulations ($r_g = 1.5$ μm) with a temperature difference of 20 K and of 120 K: consideration of crossing trajectories increases the deposition velocity, but approximately by the same amount in both cases.

The influence of thermophoresis on particle-concentration profiles is shown in Fig. 8. The sharp concentration peak near the wall is almost flattened, since particles close to the wall deposit in the presence of a strong body force (thermophoresis). A similar result was obtained in a recent study of thermophoretic deposition in a direct numerical simulation of turbulent

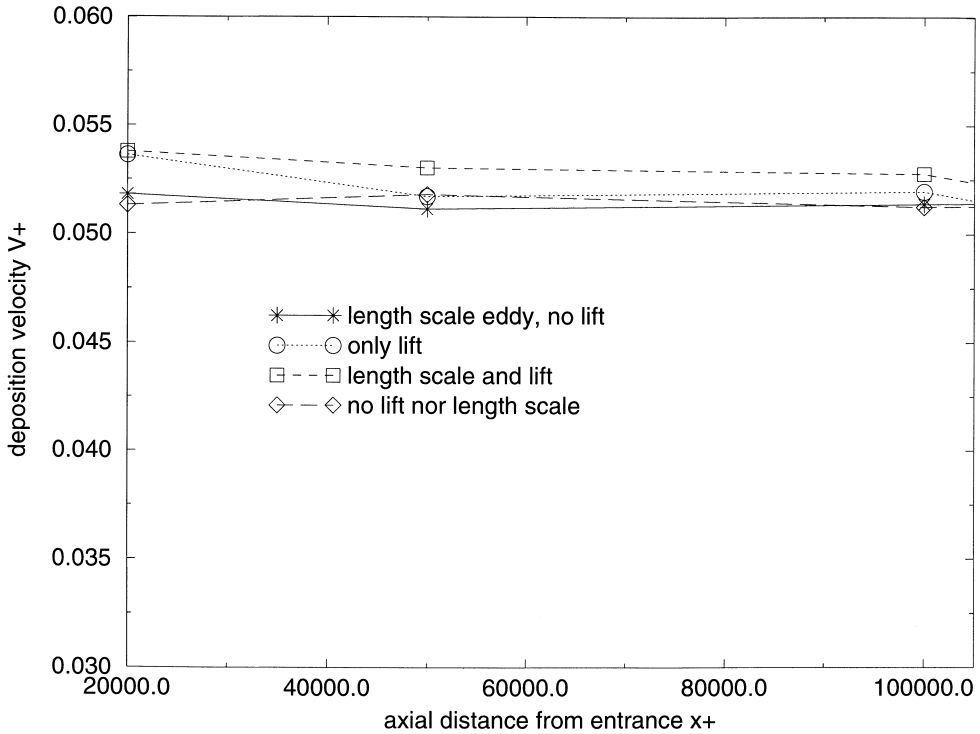

Fig. 4. Dependence of total, steady-state deposition velocity on lift and on eddy finite length scale ($r_g = 1.5$ μm, thermophoretic case).

channel flow (Thakurta et al., 1998). However, the expected increase of the wall concentration in the presence of thermophoresis (particle flux at the wall increases) is not reproduced in our simulations because the bin size was too large to obtain an accurate estimate of the wall concentration. The change of the concentration profile suggests that eddy impaction and thermophoretic deposition are not simply additive. Hence, simple addition of deposition velocities, as is usually done in one-dimensional fission product transport codes, may be in considerable error in determining total particle deposition velocities. The effect of the lift force and finite-size eddies is minimal.

The effect of thermophoresis on the particle-size distribution is presented in Fig. 9. The cumulative distribution function and the probability density function at the entrance and the exit of the pipe are determined and compared. In the absence of thermophoresis changes of the distribution function are very small, whereas in its presence a small shift to smaller particles is noted and the distribution becomes sharper; the pipe acts as a filter removing particles from both tails of the distribution.

One the main objectives of our work was the study of the effect of temperature fluctuations on particle deposition. In Fig. 10 the dimensionless deposition velocity for three sensitivity calculations is presented. All cases were run in the presence of a mean thermophoretic force. It is apparent that temperature fluctuations have a small effect on particle deposition. A similar

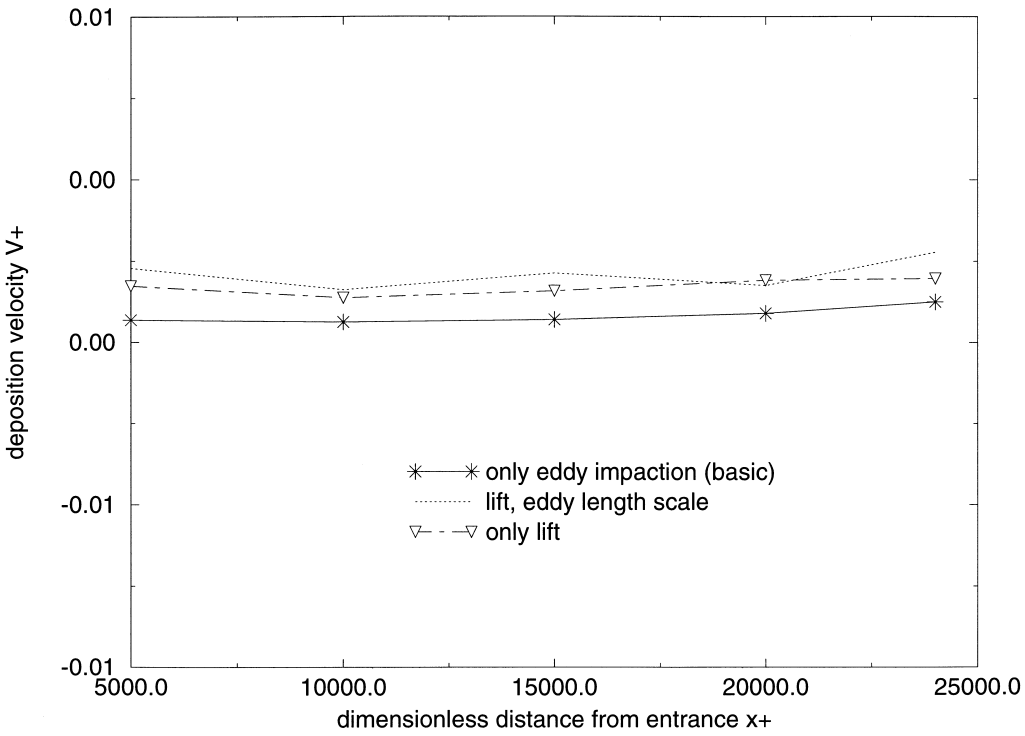

Fig. 5. Dependence of total, steady-state deposition velocity on lift and on eddy finite length scale ($r_g = 1.5$ μm, isothermal case).

conclusion was reached in the previously cited analysis of thermophoretic deposition of small particles in turbulent channel flow (Thakurta et al., 1998). Additionally, lift and reduced particle–eddy interaction time tend to increase particle deposition. Even though the effect of the fluctuating thermophoretic force is small it is comparable (for the simulated conditions) to the effect of lift and crossing trajectories. Therefore, all three effects should be included in simulations of particle deposition in heated turbulent boundary layers.

One reason for the small effect of temperature fluctuations might be the choice of the Gaussian distribution functions of zero mean for both the velocity and the temperature fields (close to the wall). It may be argued that a different choice for the distribution functions, e.g., a skewed distribution as would be expected in shear flow (Kim et al., 1987), would have a pronounced effect on particle deposition. Under the simulated conditions the mean temperature difference between the bulk gas and the wall was relatively large, but for a smaller temperature difference the effect of temperature fluctuations might become more significant for particle deposition. Finally, removal of the assumption of identical temperature and velocity distributions might have an effect on particle deposition.

Simulation results are also compared to experimental data from a typical STORM experiment, International Standard Problem ISP-40, (De Los Reyes Castelo et al., 1999). Although various effects have not been included in the model (such as resuspension, Brownian diffusion and wall roughness) results show good agreement with the experiment. Since the

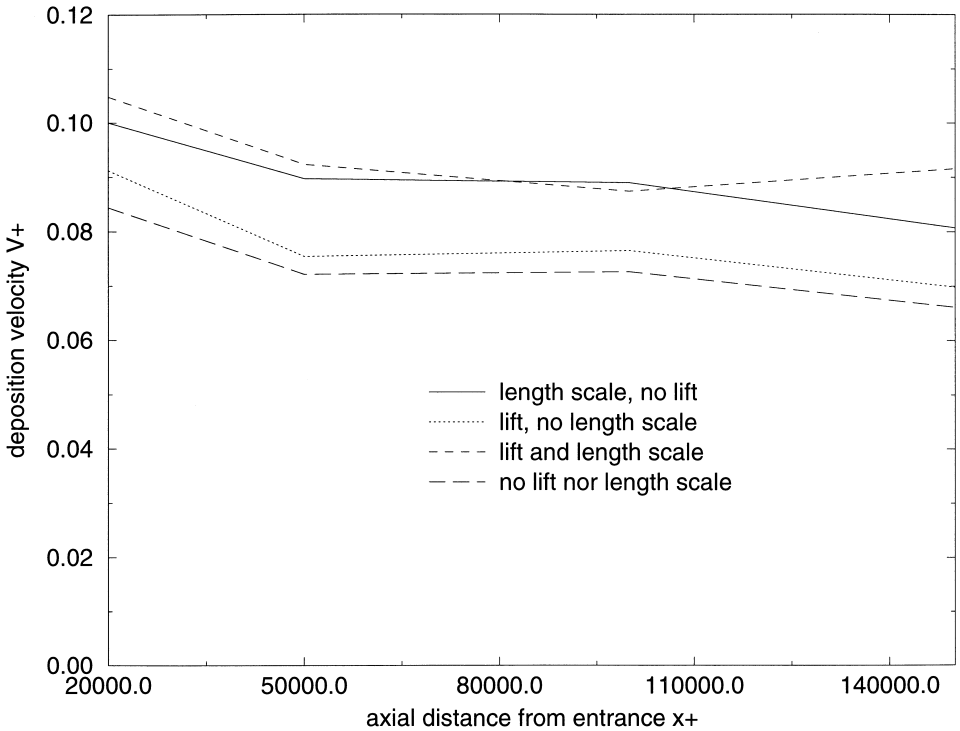

Fig. 6. Dependence of total, steady-state deposition velocity on lift and on eddy finite length scale ($r_g = 10$ μm, thermophoretic case).

aerosol had not been neutralised, electrophoresis might have had a significant contribution to particle deposition, yet the existence of a settling chamber before the deposition pipe indicates that the effect of electrical charges was minimized.

The experimental data were presented as deposited mass per unit length. The aerosol used in the experiment was tin dioxide in a steam/air/argon mixture, with an estimated particle density of 4000 kg/m^3. The corresponding deposited mass per unit length was calculated and it is compared to the experimental results in Fig. 11. Although the local simulation results are lower (at the entrance of the pipe) and higher (at the exit of the pipe) than the experimental data, the tendency is similar in both cases and the total deposited mass differs by approximately 12% (161 g experiment, 181 g calculated). The agreement is reasonable, especially in predicting the decrease in particle deposition at approximately 3 m from the entrance of the pipe (middle of pipe length). In the calculation it was assumed that the temperature gradient in the turbulent core is virtually zero, therefore, the effect of thermophoresis is restricted to the turbulent boundary layer, and hence the boundary layer model is sufficient for thermophoretic simulations. The aerosol was assumed equally distributed over the entire pipe cross section, therefore, a certain percentage of the particle flow (equal to the percentage of the boundary layer thickness to the pipe radius) was injected in the boundary layer.

Except for the Liu and Agarwal isothermal test simulations, all calculations were performed

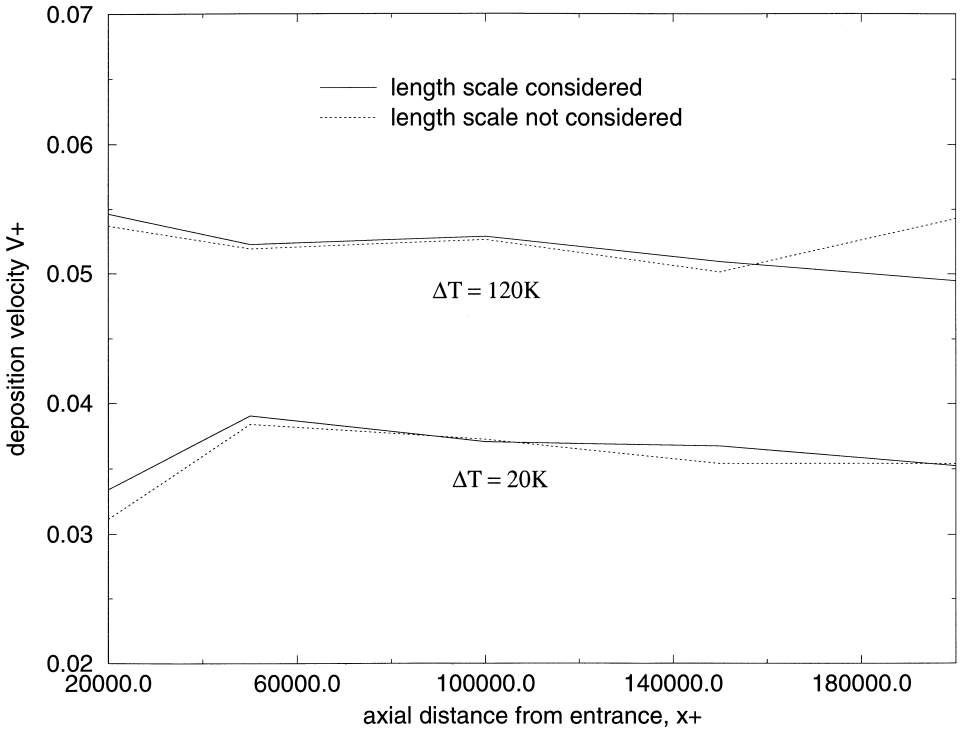

Fig. 7. Effect of crossing trajectories on particle deposition as a function of bulk to wall temperature difference ($r_g = 1.5$ μm).

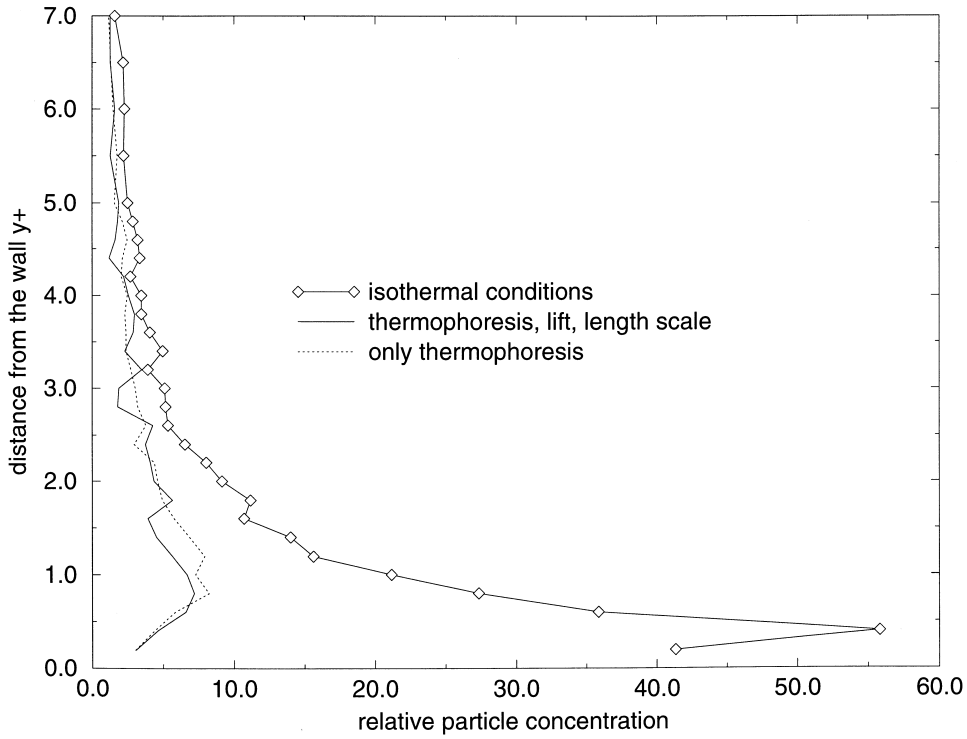

Fig. 8. Particle concentration profiles (close to the wall) in an isothermal and a heated boundary layer: temperature fluctuations neglected.

with a particle-size spectrum, rather than at a particular particle diameter. Usually 20,000 particle tracks were calculated, corresponding to approximately only 200 particle tracks in each particle size bin. A 50,000 particle tracks calculation was performed as well, but the results did not change significantly, demonstrating that steady-state conditions were obtained with 20,000 particle tracks.

5. Conclusions

Lagrangian random-walk simulations were performed to study thermophoretic particle deposition in a turbulent boundary layer. The effect of thermophoresis on particle deposition velocities and particle concentrations close to the wall was examined, and results were compared to experimental data. Emphasis was placed on the incorporation of an instantaneous temperature field, assumed to be similar to the instantaneous velocity field, and the corresponding fluctuating thermophoretic force. For the latter the r.m.s temperature gradient was chosen from a fourth-order fit to derived experimental data. Sensitivity calculations were performed on the effect of crossing trajectories and on aerodynamic lift in a heated and an isothermal flow field. The simulations were performed for a realistic particle-size spectrum,

with particle sizes ranging over approximately two orders of magnitude. A limited number of particle tracks was found sufficient for the determination of steady-state total (for all particle sizes) deposition velocity. Input data were based on experiments from the STORM experimental programme.

The code successfully reproduced the deposition velocity for single-particle sizes in an isothermal flow field (Liu and Agarwal, 1974). The introduction of a temperature gradient in the turbulent boundary layer lead to a strong increase in particle deposition. The isothermal concentration profile, which shows noticeable particle accumulation in the viscous sublayer, becomes almost flat in the presence of thermophoresis.

Crossing trajectories were determined to have a significant effect on particle deposition in the presence of strong body forces for high inertia particles, whereas their effect was negligible in isothermal cases and for particles of low inertia. For relatively small particles changes of the temperature gradient across the boundary layer did not show an increased effect of crossing trajectories on particle deposition. Therefore, in isothermal flow and for low inertia particles the particle–eddy interaction time can be set equal to the Lagrangian eddy time scale; otherwise, for particles with sufficient inertia the crossing time through the eddy should be redefined as the smaller of the crossing time and the eddy time scale, as proposed by Graham and James (1996). For the particle sizes considered (particle relaxation times in the diffusion–impaction deposition regime) the effect of Saffman lift was to increase the deposition velocity:

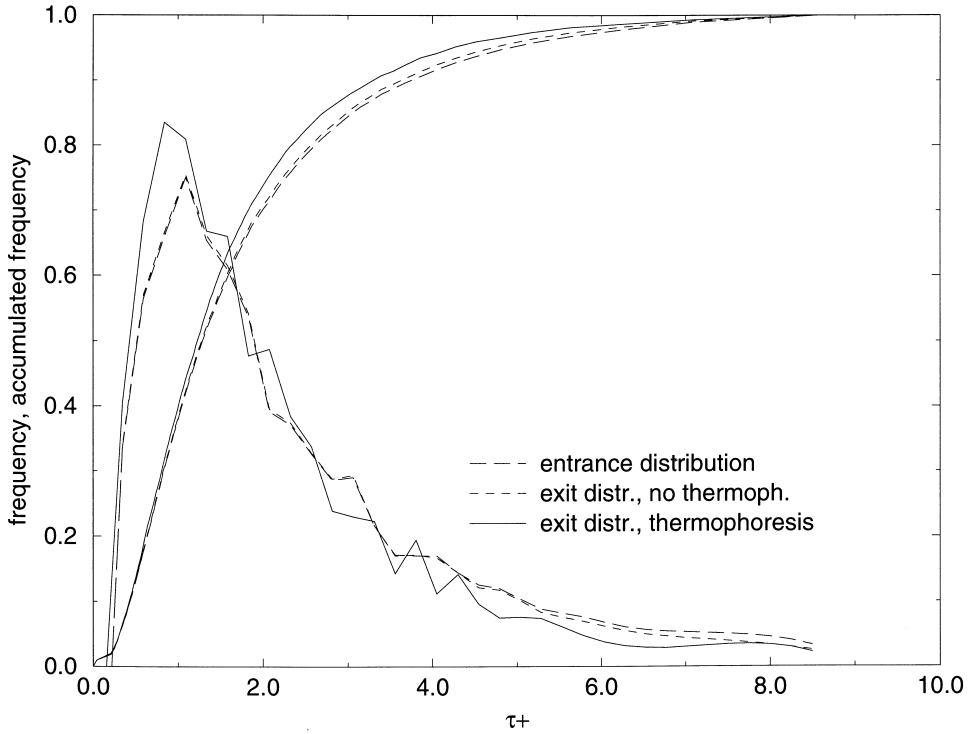

Fig. 9. Particle size distribution at the entrance and at the exit of the test section: isothermal and heated boundary layer.

however, the increase was relatively small, especially under isothermal conditions. The effect of lift and crossing trajectories on particle deposition was found to be non additive.

The effect of a fluctuating thermophoretic force on particle deposition was determined to be small, but non-negligible. Moreover, its contribution to particle deposition was comparable to that of lift and crossing trajectories. This observation suggests that in the presence of a strong temperature gradient all three effects should be considered. It remains the task of future work to determine whether the relatively small contribution of temperature fluctuations on deposition would be significantly modified if the velocity and temperature distributions were not taken to be Gaussian (for example, they may be taken to be skewed, as expected for such distributions close to the wall in a shear flow) or if these two distribution were taken to be significantly different. Similarly, a significant change in deposition velocity is expected with the inclusion of a model for bursting phenomena close to the wall.

Simulation results were compared to experimental data from the benchmark experiment ISP-40. We found that the code was capable to calculate the total deposited mass in agreement with the experiment, and to determine the location of decrease of the deposition velocity i.e., regions of higher or lower particle deposition were identified.

Our main conclusions that the mean thermophoretic force may lead to considerable increase of particle deposition, and a concomitant decrease of the concentration peak close to the wall, and that the fluctuating thermophoretic force has a little effect on the deposition velocity are in agreement with a recent calculation of thermophoretic deposition in a direct numerical

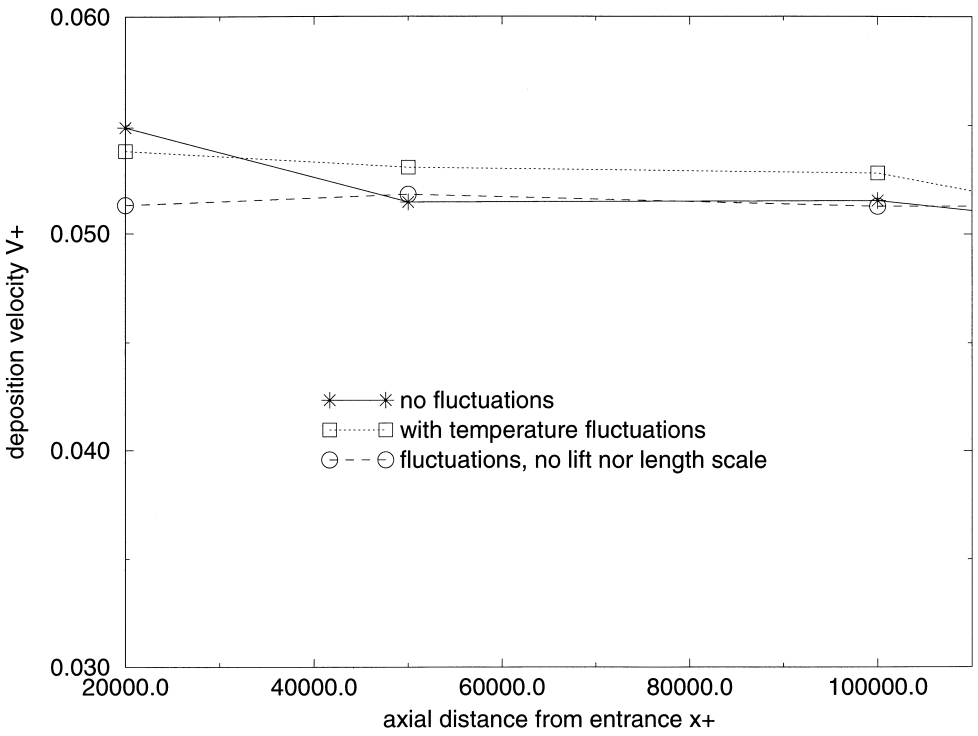

Fig. 10. Effect of temperature fluctuations on total, steady-state deposition velocity.

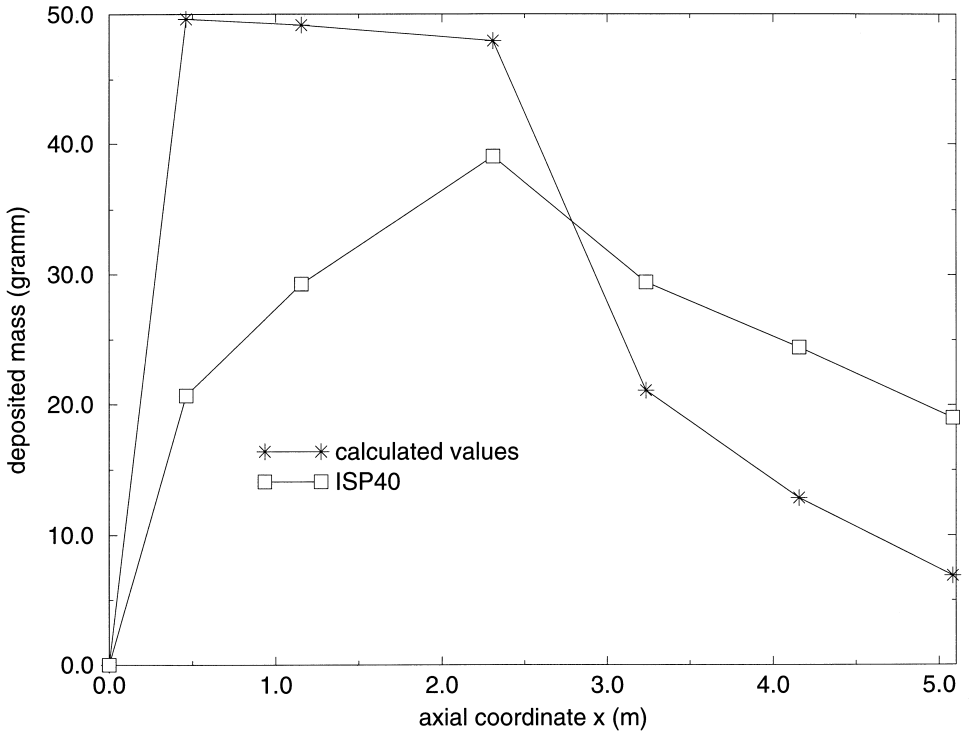

Fig. 11. Comparison of total deposited mass as a function of axial position: ISP-40 experiment and numerical simulation.

simulation of turbulent channel flow (Thakurta et al., 1998). Note, however, that the approaches used are different: a stochastic Monte-Carlo approach was used in this work to simulate the velocity and temperature fields, while the fluid flow was determined by a direct numerical simulation in Thakurta et al. (1998).

Acknowledgements

We would like to thank Mike Reeks, Joaquim Areia Capitão, Alan Jones, and the members of the STORM project for useful discussions.

References

Cherukat, P., McLaughlin, J.B., 1994. The inertial lift on a rigid sphere in a linear shear flow field near a flat wall. J. Fluid Mech 263, 1–18.

De Los Reyes Castelo, A., Areia Capitão, J., De Santi, G., 1999. International standard problem 40: aerosol deposition and resuspension. European Commission EUR 18708 EN.

De Santi, G.F., Hummel, R., Valisi, M., De Los Reyes, A., 1993. STORM project, a study on aerosol resuspension

mechanisms under prototypical severe accident conditions. In: Severe Accident Research Workshop, Tokyo, November, 1–2.
Finnicum, D.S., Hanratty, T.J., 1985. Turbulent temperature fluctuations close to a wall. Phys. Fluids 28, 1654–1658.
Graham, D.I., James, P.W., 1996. Turbulent dispersion of particle using eddy interaction models. Int. J. Multiphase Flow 22, 157–175.
Hanel, B., 19990. Einführung in die konvektive Wärme- und Stoffübertragung. Verlag Technik, Berlin.
Happel, J., Brenner, H., 1991. Low Reynolds Number Hydrodynamics. Kluwer Academic Publishers, Netherlands.
Hinds, W.C., 1982. Aerosol Technology. Wiley, New York.
Im, K.H., Ahluwalia, R.K., Chuang, C.F., 1985. RAFT: a computer code for formation and transport of fission product aerosols in LWR primary circuit. Aerosol Sci. Technol 4, 125–140.
Kallio, G.A., Reeks, M.W., 1989. A numerical simulation of particle deposition in turbulent boundary layers. Int. J. Multiphase Flow 15, 433–446.
Kennard, E.H., 1938. Kinetic Theory of Gases. McGraw-Hill, New York.
Kim, J., Moin, P., Moser, R., 1987. Turbulence statistics in fully developed channel flow at low Reynolds number. J. Fluid Mech 177, 133–166.
Krasenbrink, A., Hummel, R., Areia Capitão, J., 1996. STORM Test SD07, Deposition of tin dioxide in partially insulated pipes with steam as carrier gas. European Commission, Joint Research Centre Technical Note I.96.185.
Krishnamoorthy, L.V., Antonia, R.A., 1987. Temperature dissipation measurements in a turbulent boundary layer. J. Fluid Mech 176, 265–281.
Laufer, J., 1954. The structure of turbulence in fully developed pipe flows. NACA Report 1174, 1–18.
Lin, C.-H., Chang, L.-F.W., 1996. Analytical approach to derive the fine particle dispersion properties inherent in numerical particle trajectory models. J. Aerosol Sci 27, 618–694.
Liu, B.Y.H., Agarwal, J.K., 1974. Experimental observation of aerosol deposition in turbulent flow. J. Aerosol Sci 5, 145–155.
Lyons, S.L., Hanratty, T.J., McLaughlin, J.B., 1991. Direct numerical simulation of passive heat transfer in a turbulent channel flow. Int. J. Heat Mass Transfer 34, 1149–1161.
MacInnes, J.M., Bracco, F.V., 1992. Stochastic particle dispersion modeling and the tracer particle limit. Phys. Fluids A 4, 2809–2824.
McLaughlin, J., 1993. The lift on a small sphere in wall-bounded linear shear flows. J. Fluid Mech 246, 249–265.
Mollinger, A.M., Nieuwstadt, F.T.M., 1996. Measurement of the lift force on a particle fixed to the wall in the viscous sublayer of a fully developed turbulent boundary layer. J. Fluid Mech 316, 285–306.
Press, W.H., Flannery, B.P., Teukolsky, S.A., Vetterling, W.T., 1995. Numerical Recipes in C, 2nd ed. Cambridge University Press, Cambridge.
Reeks, M.W., 1977. On the dispersion of small particles suspended in an isotropic turbulent fluid. J. Fluid Mech 83, 529–546.
Saffman, P.G., 1965. The lift on a small sphere in a slow shear flow. J. Fluid Mech 22, 385–400.
Saffman, P.G., 1968. Corrigendum to The lift on a small sphere in a slow shear flow. J. Fluid Mech 31, 624.
Schlichting, H., 1979. Boundary-Layer Theory. McGraw-Hill, New York.
Tanimoto, S., Hanratty, T.J., 1963. Fluid temperature fluctuations accompanying turbulent heat transfer in a pipe. Chem. Engng. Sci 18, 307–311.
Talbot, L., Cheng, R., Schefer, R., Willis, D., 1980. Thermophoresis of particles in a heated boundary layer. J. Fluid Mech 101, 737–758.
Thakurta, D.G., Chen, M., McLaughlin, J.B., Kontomaris, K., 1998. Thermophoretic deposition of small particles in a direct numerical simulation of turbulent channel flow. Int. J. Heat Mass Transfer 41, 4167–4182.
Wang, Q., Squires, K.D., Chen, M., McLaughlin, J.B., 1997. On the role of the lift force in turbulence simulations of particle deposition. Int. J. Multiphase Flow 23, 749–763.
Wei, T., Wilmarth, 1989. Reynolds number effects on the structure of a turbulent channel flow. J. Fluid Mech. 204, 57–95.
Wells, M.R., Stock, D.E., 1983. The effect of crossing trajectories on the dispersion of particles in turbulent flow. J. Fluid Mech 136, 31–62.
Wilson, J.D., Thurtell, G.W., Kidd, G.E., 1980. Numerical simulation of particle trajectories in inhomogeneous

turbulence, II: Comparison of predictions with experimental data for the atmospheric surface layer. Boundary-Layer Meteorology 21, 443–463.
Wilson, J.D., Thurtell, G.W., Kidd, G.E., 1981. Numerical simulation of particle trajectories in inhomogeneous turbulence, I: Systems with variable turbulent velocity scale. Boundary-Layer Meteorology 21, 423–441.
Young, J., Leeming, A., 1997. A theory of particle deposition in turbulent pipe flow. J. Fluid Mech 340, 129–159.
Zumwalt, L.C., Kallio, G., 1990. A numerical simulation of thermophoretic deposition in turbulent flow. Proceedings Spring Meeting ASME Fluids Engineering, FED 91, 1–9.